

# Area and Length Minimizing Flows for Shape Segmentation \*

Kaleem Siddiqi<sup>†</sup>    Yves Bérubé Lauzière<sup>‡</sup>    Allen Tannenbaum<sup>§</sup>  
Steven W. Zucker<sup>†</sup>

<sup>†</sup>Center for Computational Vision & Control  
Yale University, New Haven, CT 06520-8285  
{siddiqi-kaleem,zucker-steven}@cs.yale.edu

<sup>‡</sup>Center for Intelligent Machines  
McGill University, Montréal, PQ H3A 2A7, Canada  
berube@cim.mcgill.ca

<sup>§</sup>Dept. of Electrical Engineering  
University of Minnesota, Minneapolis, MN 55455  
tannenba@ee.umn.edu

CVC TR-97-001/CS TR-1146

February, 1997

---

\*To Appear in the IEEE Transactions on Image Processing.

## Abstract

A number of active contour models have been proposed which unify the curve evolution framework with classical energy minimization techniques for segmentation, such as snakes. The essential idea is to evolve a curve (in 2D) or a surface (in 3D) under constraints from image forces so that it clings to features of interest in an intensity image. Recently the evolution equation has been derived from first principles as the gradient flow that minimizes a modified length functional, tailored to features such as edges. However, because the flow may be slow to converge in practice, a constant (hyperbolic) term is added to keep the curve/surface moving in the desired direction. In this paper, we derive a modification of this term based on the gradient flow derived from a weighted area functional, with image dependent weighting factor. When combined with the earlier modified length gradient flow we obtain a pde which offers a number of advantages, as illustrated by several examples of shape segmentation on medical images. In many cases the weighted area flow may be used on its own, with significant computational savings.

**Keywords:** Curve evolution, snakes, edge capturing, gradient flows.

## 1 Introduction

In the application of curve evolution theory to visual shape analysis, Kimia, Tannenbaum and Zucker introduced a reaction-diffusion space for shape representation [16, 18, 17]. Using a reaction-diffusion model from mathematical physics a planar shape is evolved with a velocity vector in the direction normal to the moving front, which consists of two terms: a constant (hyperbolic) term, and a curvature (parabolic) term. The key idea is to play off one term against the other: the constant motion term leads to the formation of shocks from which a representation of shape can be derived, and the diffusive curvature term smoothes the front, which is essential for distinguishing more significant shape features from less significant ones.

This type of technique was introduced into shape modelling by Casselles *et al.* [7] and Malladi *et al.* [19], via the addition of a multiplicative image gradient stopping term. This has led to powerful new techniques for edge capturing. These active contour models have the significant advantage over classical snakes that changes in topology due to the splitting and merging of multiple contours,

are handled in a natural way. Along these lines, Tek and Kimia [28] have further suggested a reaction-diffusion space of bubbles, where in place of a single contour, a number of bubbles are simultaneously placed and grown from homogeneous regions of the image.

Against this background, in several independent works [8, 13, 14, 26] a new active contour model was proposed which unified the curve evolution approaches with the classical energy minimization methods [12, 29, 5]. The technique is motivated by the Euclidean curve shortening equation which defines the gradient direction in which the Euclidean perimeter is shrinking as fast as possible. The key insight is to multiply the Euclidean arc-length by a function tailored to the features of interest in the intensity image, and then to write down the resulting *gradient evolution equations*. Mathematically, this amounts to defining a new metric in the plane tailored to the given image, and then computing the corresponding gradient flow. This leads to new snake models which efficiently attract the evolving front to features such as edges. A viscosity analysis of the evolution equation demonstrates the existence and uniqueness of a solution to the partial differential equation and provides theoretical justification for its use.

Whereas the above method motivates the use of a curvature term in shape modelling, the flow can be unacceptably slow to converge in practice. Therefore, the authors of [8, 13, 14, 26] follow [7, 19] by adding a constant inflation term to keep the curve moving in the desired direction. Our main contribution in this paper is the modification of this hyperbolic term with one derived from minimizing a certain weighted area energy functional. More precisely, in analogy to the case of Euclidean arc-length we modify the infinitesimal Euclidean area by a conformal factor and compute the gradient flow for the modified area functional. The derived flow turns out to have two components, one which is constant and one which depends on the conformal factor as well as the evolving curve. When combined with the weighted length minimizing flow derived in [8, 13, 14, 26], we obtain a partial differential equation whose parabolic and hyperbolic components each have consistent interpretations as gradient flows.

In application to shape segmentation the new flow exhibits a stronger attraction force to features of interest than the constant inflation term previously used, due to the inclusion of a new doublet term. In fact, in several numerical experiments we found the conformal area flow to be sufficient to segment the image. Since this flow requires the computation of only first-order derivatives, it offers significant computational savings over the weighted length minimizing flow.

As an aside we should add that our original interest in deriving the weighted area flow was in

application to shape analysis following [16, 18, 17]. The difficulty with employing that reaction-diffusion model directly is that the slightest bit of diffusion tends to dominate, preventing the formation of generic first-order shocks which are key to shape representation. In a separate paper [27], we will show how to design the conformal factor in the weighted area flow such that the pde initially mimics parabolic behavior (allowing for degrees of smoothing) but later becomes a pure constant motion flow leading to the formation of the generic shocks of the pure reaction axis, which are equivalent to Blum’s skeleton.

The paper is organized as follows. In Section 2 we review the relationship between the two components of the reaction-diffusion model and gradient flows, present the evolution equation of the weighted length minimizing flow derived in [8, 13, 14, 26], and then introduce and derive the weighted area minimizing gradient flow. In Section 3 we review the level set representation for curves flowing according to functions of curvature due to Osher and Sethian [21, 23, 24, 25], which is the basis of their numerical algorithm for simulation which we utilize. In Section 4 we review the past work on shape modelling and propose our new evolution equation, the linear combination of the weighted length and weighted area gradient flows. We further show how our models may be easily extended to the 3D case in Section 5. In Section 6 we present several numerical simulations that illustrate the advantages of the new flow for edge capturing. Finally in Section 7, we briefly summarize our results, and discuss some future work.

## 2 Weighted Gradient Flows

The foundation of our approach is the mathematical theory of curves flowing in the plane with speed a function of curvature. In [16, 18, 17], the two key components of this motion were combined into a reaction-diffusion space for shape analysis. More precisely with  $\kappa$  the curvature,  $\mathcal{N}$  the inward unit normal, and  $\mathcal{C}$  the curve coordinates, consider families of plane curves flowing according the equation

$$\frac{\partial \mathcal{C}}{\partial t} = (\alpha + \beta \kappa) \mathcal{N} \tag{1}$$

where  $\alpha, \beta \in \mathbf{R}$ ,  $\beta \geq 0$ . In this section we shall examine the weighted generalizations of the two parts of this evolution.

## 2.1 Curvature Motion

Referring to Eq. 1, we take  $\alpha = 0, \beta = 1$ , and so we get the family of plane curves flowing according to the *geometric heat equation*

$$\frac{\partial \mathcal{C}}{\partial t} = \kappa \mathcal{N}. \quad (2)$$

This equation has a number of properties which make it very useful in image processing. In particular, (2) is the Euclidean curve shortening flow, in the sense that the Euclidean perimeter shrinks as quickly as possible when the curve evolves according to (2) [10, 11]. Since we will need a similar argument for subsequent models, let us work out the details.

Let  $\mathcal{C} = \mathcal{C}(p, t)$  be a smooth family of closed curves where  $t$  parametrizes the family and  $p$  the given curve, say  $0 \leq p \leq 1$ . (Note we assume that  $\mathcal{C}(0, t) = \mathcal{C}(1, t)$  and similarly for the first derivatives.) Define the length functional

$$L(t) = \int_0^1 \left\| \frac{\partial \mathcal{C}}{\partial p} \right\| dp.$$

Differentiating (taking the “first variation” with respect to  $t$ ), and using integration by parts, one can show that

$$L'(t) = - \int_0^{L(t)} \left\langle \frac{\partial \mathcal{C}}{\partial t}, \kappa \mathcal{N} \right\rangle ds,$$

where  $ds = \left\| \frac{\partial \mathcal{C}}{\partial p} \right\| dp$  denotes arc-length. Thus the direction in which  $L(t)$  is decreasing most rapidly is when  $\frac{\partial \mathcal{C}}{\partial t} = \kappa \mathcal{N}$ . Thus (2) defines a *gradient flow*.

A much deeper fact is that simple closed curves converge to “round” points when evolving according to (2) without developing singularities. This means that if we consider an associated family of dilated curves of constant area (look at the evolving family of shrinking curves under a “magnifying glass”), the curves of the family approach a circle; see [10, 11]. This fact is the basis for the nonlinear geometric scale-spaces studied recently in [2, 1, 16, 18].

## 2.2 Weighted Length Gradient Flows

In the recent papers [8, 13, 14, 26], the standard Euclidean metric  $ds^2 = dx^2 + dy^2$  of the underlying space over which the evolution takes place is modified to a conformal metric  $ds_\phi^2 = \phi^2(dx^2 + dy^2)$ .

Using this metric, the “ $\phi$ -length” of the curve is defined as

$$L_\phi(t) = \int_0^1 \left\| \frac{\partial \mathcal{C}}{\partial p} \right\| \phi dp. \quad (3)$$

Here  $\phi : \mathbf{R}^2 \rightarrow \mathbf{R}$  is a positive differentiable function defined on the image plane. By requiring the  $\phi$ -length to shrink as quickly as possible, the following flow is obtained

$$\boxed{\mathcal{C}_t = \{\phi\kappa - \nabla\phi \cdot \mathcal{N}\}\mathcal{N}.} \quad (4)$$

Note that this last equation consists of two terms. The first is the curvature term of equation (2) multiplied by  $\phi$ , and the second depends on the gradient of the conformal factor. In application to shape modelling the latter term acts like a doublet which attracts the active contour to the feature of interest. We will now treat the constant speed term of the reaction-diffusion model in the same way.

### 2.3 Constant Motion

Again, referring to equation (1), we take  $\alpha = 1$ ,  $\beta = 0$ , which gives the constant motion flow

$$\mathcal{C}_t = \mathcal{N}. \quad (5)$$

In analogy to the geometric heat equation which minimizes Euclidean length, this evolution may be derived as the gradient flow which locally minimizes area. Indeed, for the family of closed curves defined above, the area functional is given by

$$A(t) = -\frac{1}{2} \int_0^L \langle \mathcal{C}, \mathcal{N} \rangle ds = -\frac{1}{2} \int_0^1 \langle \mathcal{C}, \begin{pmatrix} -y_p \\ x_p \end{pmatrix} \rangle dp.$$

Again, taking the first variation

$$A'(t) = -\frac{1}{2} \int_0^1 \langle \mathcal{C}_t, \begin{pmatrix} -y_p \\ x_p \end{pmatrix} \rangle dp - \frac{1}{2} \int_0^1 \langle \mathcal{C}, \begin{pmatrix} -y_{pt} \\ x_{pt} \end{pmatrix} \rangle dp.$$

Using integration by parts for the second integral and changing to arc-length parametrization

$$A'(t) = - \int_0^L \langle \mathcal{C}_t, \mathcal{N} \rangle ds.$$

Thus the direction in which  $A(t)$  is decreasing most rapidly (locally) is when  $\mathcal{C}_t = \mathcal{N}$  and (5) also defines a *gradient flow*.

**Remark.**

It is important to note that equations (2) and (5) are guaranteed to give the direction of maximal

decrease of their respective functional only locally. Global existence results are much deeper. In fact, we have already stated that a smooth embedded curve shrinking under (2) remains regular, that is this flow is indeed smoothing. The constant motion flow (5) on the other hand can cause a smooth curve to evolve to a singular one. In fact, this is one of its desirable characteristics since the resulting shocks are important features for the computational theory of shape in [16, 18, 17].

## 2.4 Weighted Area Gradient Flows

Our strategy, in analogy to what has been done for length, is to consider area in the conformal metric. Hence our starting point is the modified area functional

$$A_\phi(t) = -\frac{1}{2} \int_0^{L(t)} \phi \langle \mathcal{C}, \mathcal{N} \rangle ds = -\frac{1}{2} \int_0^1 \phi \left\langle \mathcal{C}, \begin{pmatrix} -y_p \\ x_p \end{pmatrix} \right\rangle dp.$$

Here  $\phi : \mathbf{R}^2 \rightarrow \mathbf{R}$  is a positive differentiable function defined on the image plane. We now derive the flow associated with the  $\phi$ -area,  $A_\phi$ . As above, differentiating the functional with respect to  $t$  will give us the evolution equation for the curve:

$$-2A'_\phi(t) = I_1 + I_2 + I_3$$

with

$$\begin{aligned} I_1 &= \int_0^L \langle \nabla \phi, \mathcal{C}_t \rangle \langle \mathcal{C}, \mathcal{N} \rangle ds, \\ I_2 &= \int_0^L \phi \langle \mathcal{C}_t, \mathcal{N} \rangle ds, \\ I_3 &= \int_0^1 \left\langle \phi \mathcal{C}, \begin{pmatrix} -y_{pt} \\ x_{pt} \end{pmatrix} \right\rangle dp. \end{aligned}$$

For  $I_3$  using integration by parts, we get

$$I_3 = - \int_0^1 \left\langle (\phi \mathcal{C})_p, \begin{pmatrix} -y_t \\ x_t \end{pmatrix} \right\rangle dp.$$

We will use the following notation: let  $V = (a, b)$  be a vector, its “perp” is defined by

$$V^\perp = (-b, a).$$

With respect to the scalar product we have the following properties

$$\begin{aligned}\langle V_1, V_2^\perp \rangle &= -\langle V_1^\perp, V_2 \rangle \\ \langle V_1^\perp, V_2^\perp \rangle &= \langle V_1, V_2 \rangle.\end{aligned}\tag{6}$$

Using this, we rewrite  $I_3$  as follows

$$\begin{aligned}I_3 &= -\int_0^1 \langle (\phi \mathcal{C})_p, (\mathcal{C}_t)^\perp \rangle dp \\ &= \int_0^1 \langle \mathcal{C}_t, (\phi \mathcal{C})_p^\perp \rangle dp.\end{aligned}$$

But

$$\begin{aligned}(\phi \mathcal{C})_p &= \langle \nabla \phi, \mathcal{C}_p \rangle \mathcal{C} + \phi \mathcal{C}_p \\ \Rightarrow (\phi \mathcal{C})_p^\perp &= \langle \nabla \phi, \mathcal{C}_p \rangle \mathcal{C}^\perp + \phi \mathcal{C}_p^\perp,\end{aligned}$$

hence

$$\begin{aligned}I_3 &= \int_0^1 \langle \mathcal{C}_t, \langle \nabla \phi, \mathcal{C}_p \rangle \mathcal{C}^\perp + \phi \mathcal{C}_p^\perp \rangle dp \\ &= \int_0^1 \langle \nabla \phi, \mathcal{C}_p \rangle \langle \mathcal{C}_t, \mathcal{C}^\perp \rangle dp + \int_0^1 \phi \langle \mathcal{C}_t, \mathcal{C}_p^\perp \rangle dp.\end{aligned}$$

Using equation (6) this can be rewritten as

$$I_3 = \int_0^1 \langle \mathcal{C}_t, \mathcal{C}^\perp \rangle \langle \nabla \phi^\perp, \mathcal{C}_p^\perp \rangle dp + \int_0^1 \phi \langle \mathcal{C}_t, \mathcal{C}_p^\perp \rangle dp,$$

and finally changing to arc length parametrization

$$I_3 = \int_0^L \langle \mathcal{C}_t, \mathcal{C}^\perp \rangle \langle \nabla \phi^\perp, \mathcal{N} \rangle ds + \int_0^L \phi \langle \mathcal{C}_t, \mathcal{C}^\perp \rangle ds.$$

Grouping everything together, we get

$$-2A'_\phi(t) = \int_0^L \langle \mathcal{C}_t, \langle \mathcal{C}, \mathcal{N} \rangle \nabla \phi + 2\phi \mathcal{N} + \langle \nabla \phi^\perp, \mathcal{N} \rangle \mathcal{C}^\perp \rangle ds.$$

Therefore for  $A_\phi$  to decrease as fast as possible, take

$$\mathcal{C}_t = \phi \mathcal{N} + \frac{1}{2} \left[ \langle \mathcal{C}, \mathcal{N} \rangle \nabla \phi + \langle \nabla \phi^\perp, \mathcal{N} \rangle \mathcal{C}^\perp \right].$$

Now decomposing  $\nabla \phi$  and  $\mathcal{C}^\perp$  in the Frenet frame  $\{T, \mathcal{N}\}$ , and dropping the tangential terms, which can always be done by reparametrizing the curve, we end up with

$$\mathcal{C}_t = \left\{ \phi + \frac{1}{2} \left[ \langle \nabla \phi, \mathcal{N} \rangle \langle \mathcal{C}, \mathcal{N} \rangle + \langle \nabla \phi^\perp, \mathcal{N} \rangle \langle \mathcal{C}^\perp, \mathcal{N} \rangle \right] \right\} \mathcal{N}.$$

The last result can be simplified further. Writing  $\nabla\phi = (\phi_x, \phi_y)$ ,  $\mathcal{C}(p, t) = (x(p, t), y(p, t))$  and expanding the scalar products we obtain

$$\langle \nabla\phi, \mathcal{N} \rangle \langle \mathcal{C}, \mathcal{N} \rangle + \langle \nabla\phi^\perp, \mathcal{N} \rangle \langle \mathcal{C}^\perp, \mathcal{N} \rangle = \langle \mathcal{C}, \nabla\phi \rangle.$$

Hence the  $\phi$ -area minimizing evolution equation takes on the following simple form

$$\boxed{\mathcal{C}_t = \left\{ \phi + \frac{1}{2} \langle \mathcal{C}, \nabla\phi \rangle \right\} \mathcal{N}.} \quad (7)$$

Note that since  $\phi$  is a globally defined function on the image plane, (7) defines a hyperbolic equation.

**Remarks.**

(1) It is very interesting to note that minimizing the area functional in an affine sense leads to the affine curve shortening flow introduced in [1, 22]; see [20] for the details. If the area functional is modified by a stopping term, and the minimizing flow is computed again in this affine invariant sense, one gets an affine invariant snake model based on  $\kappa^{1/3}$ , [20]. This is the affine analogue of the work in [8, 13, 14, 26].

In the present work, we are modifying the area functional in the usual Euclidean  $L^2$  sense which leads to the hyperbolic equation (7).

(2) As pointed out by the referee, an equation of the form

$$\mathcal{C}_t = \psi \mathcal{N}, \quad (8)$$

may be derived by minimizing a weighted area functional of the form

$$\int \psi \, dx dy.$$

Via Green's theorem, this is equivalent to minimizing the modified area function  $A_\phi(t)$  proposed above. In fact using Green's theorem, we have that

$$A_\phi(t) = -\frac{1}{2} \int_0^{L(t)} \phi \langle \mathcal{C}, \mathcal{N} \rangle ds = \frac{1}{2} \iint \operatorname{div} \left( \begin{pmatrix} x \\ y \end{pmatrix} \phi \right) dx dy.$$

Thus for given  $\psi$ , we may find  $\phi$ , by solving

$$\psi = \frac{1}{2} \operatorname{div} \left( \begin{pmatrix} x \\ y \end{pmatrix} \phi \right),$$

and conversely.

We believe however that writing the weighted flow in the form (7) and using the functional  $A_\phi$  offers a number of important advantages, most important of which is the explicit doublet term  $\langle \mathcal{C}, \nabla \phi \rangle$  which has the effect of stopping the evolving contour at an edge, as we will subsequently see.

### 3 Level Set Representations

In this section we review the level set representation for curves flowing according to functions of curvature, due to Osher and Sethian [21, 24, 25], which is the basis for their numerical algorithm for curve (and hypersurface) evolution which we utilize. Let  $\mathcal{C}(p, t) : S^1 \times [0, \tau) \rightarrow \mathbf{R}^2$  be a family of curves satisfying the following evolution equation:

$$\frac{\partial \mathcal{C}}{\partial t} = S \mathcal{N}. \quad (9)$$

The curve  $\mathcal{C}(p, t)$  is represented by the zero level set of a smooth and Lipschitz continuous function  $\Psi : \mathbf{R}^2 \times [0, \tau) \rightarrow \mathbf{R}$ , given by  $\{X \in \mathbf{R}^2 : \Psi(X, t) = 0\}$ . Since  $\mathcal{C}(p, t)$  is on the zero level set, it satisfies

$$\Psi(\mathcal{C}, t) = 0. \quad (10)$$

By differentiating (10) with respect to  $t$ , and then with respect to the curve parameter  $p$ , it can be shown that

$$\Psi_t = S \|\nabla \Psi\|. \quad (11)$$

Equation (11) is solved using a combination of straightforward discretization and numerical techniques derived from hyperbolic conservation laws. The curve  $\mathcal{C}$ , evolving according to (9), is then obtained as the zero level set of  $\Psi$ . As an example, noting that

$$\phi + \frac{1}{2}(x\phi_x + y\phi_y) = \frac{1}{2}\text{div} \left( \begin{pmatrix} x \\ y \end{pmatrix} \phi \right), \quad (12)$$

the level set representation of the  $\phi$ -area minimizing flow (7) is given by

$$\boxed{\Psi_t = \frac{1}{2}\text{div} \left( \begin{pmatrix} x \\ y \end{pmatrix} \phi \right) \|\nabla \Psi\|}. \quad (13)$$

Similarly, the  $\phi$ -length minimizing flow (4) in level set form is

$$\boxed{\Psi_t = \left( \phi\kappa + \langle \nabla\phi, \frac{\nabla\Psi}{\|\nabla\Psi\|} \rangle \right) \|\nabla\Psi\| .} \quad (14)$$

## 4 Shape Modelling

In this section we propose the application of a combined length and area minimizing flow to the problem of shape segmentation. We begin with a brief review of earlier work in the area. Caselles *et al.* [7] and Malladi *et al.* [19] proposed an active contour model based on the following level set formulation:

$$\Psi_t = \phi(x, y) \left( \operatorname{div} \left( \frac{\nabla\Psi}{\|\nabla\Psi\|} \right) + \nu \right) \|\nabla\Psi\| . \quad (15)$$

Here the potential  $\phi(x, y)$  is constructed to have local minima at edges so that the evolving curve stops at them. For example, in [7, 19]  $\phi(x, y)$  takes the form:

$$\phi = \frac{1}{1 + \|\nabla G_\sigma * I\|^n} \quad (16)$$

where  $I$  is the grey-scale image and  $G_\sigma$  is a Gaussian smoothing filter. Building upon this work, Tek and Kimia suggested a reaction-diffusion space of bubbles [28] where the key idea is to randomly initialize a number of “seeds,” instead of a single contour. This allows for multiple structures to be captured, such as objects with holes.

It is important to note that in the above methods, the Euclidean curve shortening part of the evolution equation is the gradient flow for shrinking the perimeter of the curve as fast possible; Section 2. As explained earlier, in [8, 26, 13, 14] this model is revised and given theoretical justification by replacing the Euclidean metric  $ds^2 = dx^2 + dy^2$  with the conformal metric  $ds_\phi^2 = \phi^2(dx^2 + dy^2)$  and deriving the associated  $\phi$ -length gradient flow. In the resulting evolution equation (14) the second term  $\langle \nabla\phi, \nabla\Psi \rangle$  acts as a doublet, attracting the curve when it is in the vicinity of an edge<sup>1</sup>. Nevertheless, the flow suffers from the practical limitation that the simulation can be extremely slow to converge. As a remedy, the authors of [8, 26, 13, 14] follow [7, 19] by adding a constant (hyperbolic) term to keep the curve moving in the desired direction. The calculation of Section 2

---

<sup>1</sup>In fact due to the doublet the front will pass back and forth across the edge, but will not stray from it. In contrast in the earlier methods which rely on Eq. 15 the front will eventually pass through and move away from the edge.

suggests the modification of replacing the hyperbolic term with the  $\phi$ -area minimizing flow. The combined equation in level set form is given by:

$$\Psi_t = \underbrace{\left[ \alpha \left( \phi \kappa + \left\langle \nabla \phi, \frac{\nabla \Psi}{\|\nabla \Psi\|} \right\rangle \right) \|\nabla \Psi\| \right]}_{\phi\text{-length}} + \underbrace{\left[ \frac{1}{2} \operatorname{div} \left( \begin{pmatrix} x \\ y \end{pmatrix} \phi \right) \|\nabla \Psi\| \right]}_{\phi\text{-area}}. \quad (17)$$

Note that we have put in a “fudge” factor  $\alpha$  in order to make the units compatible (area and length cannot be added) in (17). Since  $\phi$  is a globally defined function which depends on the given image, the  $\phi$ -area part indeed defines a Hamilton-Jacobi equation. Notice by equation (12) that this  $\phi$ -area minimizing component provides the constant inflationary term (with  $\nu = 1$ ) used in the earlier approaches to shape modelling [7, 19, 28, 8, 13, 14, 26], as well as a second doublet term which provides an additional attraction force when the front is in the vicinity of an edge. We will illustrate the application of (17) with several numerical simulations of shape segmentation in Section 6.

## 5 Volumetric Extensions

In this section we develop the 3-D extension of our model, by modifying the Euclidean volume in this case by a function which depends on the salient features which we wish to capture. In order to do this, we will need to set up some notation. (For all the relevant concepts on the differential geometry of surfaces, we refer the reader to [6].)

Let  $\mathcal{S} : [0, 1] \times [0, 1] \rightarrow \mathbf{R}^3$  denote a compact embedded surface with (local) coordinates  $(u, v)$ . Let  $H$  denote the mean curvature and  $\mathcal{N}$  the inward unit normal. We set

$$\mathcal{S}_u := \frac{\partial \mathcal{S}}{\partial u}, \quad \mathcal{S}_v := \frac{\partial \mathcal{S}}{\partial v}.$$

Then the infinitesimal area on  $\mathcal{S}$  is given by

$$d\mathcal{S} = (\|\mathcal{S}_u\|^2 \|\mathcal{S}_v\|^2 - \langle \mathcal{S}_u, \mathcal{S}_v \rangle^2)^{1/2} du dv.$$

Let  $\phi : \Omega \rightarrow \mathbf{R}$  be a positive differentiable function defined on some open subset of  $\mathbf{R}^3$ . The function  $\phi(x, y, z)$  will play the role of the “stopping” function  $\phi$  given above in the 2D case. By considering the volume functional

$$V(t) := -1/3 \int \langle \mathcal{S}, \mathcal{N} \rangle d\mathcal{S},$$

and using integration by parts and standard properties of the cross product from vector calculus, it is easy to show that

$$V'(t) := - \int \langle \mathcal{S}_t, \mathcal{N} \rangle d\mathcal{S}.$$

Hence the direction in which volume is shrinking most rapidly (using only local information) is given by

$$\mathcal{S}_t = \mathcal{N}.$$

As above, we modify  $d\mathcal{S}$  in the following manner:

$$d\mathcal{S}_\phi := \phi d\mathcal{S}.$$

Then, if we consider the modified volume functional

$$V_\phi(t) := -1/3 \int \phi \langle \mathcal{S}, \mathcal{N} \rangle d\mathcal{S},$$

and perform a similar computation, we get that

$$\boxed{\mathcal{S}_t = \left\{ \phi + \frac{1}{3} \langle \mathcal{S}, \nabla \phi \rangle \right\} \mathcal{N}.} \quad (18)$$

The level set version of this may be computed to be

$$\boxed{\Psi_t = \frac{1}{3} \operatorname{div} \left( \begin{pmatrix} x \\ y \\ z \end{pmatrix} \phi \right) \|\nabla \Psi\|.} \quad (19)$$

Now the 3D extension of (4) was derived in [13, 14, 30, 9] as

$$\frac{\partial \mathcal{S}}{\partial t} = \phi H \mathcal{N} - \nabla \phi. \quad (20)$$

The level set version of (20) is given in terms of  $\Psi(x, y, z, t)$  by

$$\Psi_t = \left( \phi \operatorname{div} \left( \frac{\nabla \Psi}{\|\nabla \Psi\|} \right) + \langle \nabla \phi, \frac{\nabla \Psi}{\|\nabla \Psi\|} \rangle \right) \|\nabla \Psi\|. \quad (21)$$

Therefore, putting the two flows together we get the three dimensional extension of (17):

$$\Psi_t = \underbrace{\left[ \alpha \left\{ \phi \operatorname{div} \left( \frac{\nabla \Psi}{\|\nabla \Psi\|} \right) + \langle \nabla \phi, \frac{\nabla \Psi}{\|\nabla \Psi\|} \rangle \right\} \|\nabla \Psi\| \right]}_{\phi\text{-surface-area}} + \underbrace{\left[ \frac{1}{3} \operatorname{div} \left( \begin{pmatrix} x \\ y \\ z \end{pmatrix} \phi \right) \|\nabla \Psi\| \right]}_{\phi\text{-volume}}. \quad (22)$$



Figure 1: The original images: a 256x256 MRI slice of a brain (LEFT), a 256x256 MRI short axis view of a heart (MIDDLE), and a 276x268 CT bone image (RIGHT).

Note that we have again put in a “fudge” factor  $\alpha$  in order to get compatible units in the sum on the right side of (22). Obviously the argument extends to hypersurfaces in  $\mathbf{R}^n$ .

**Remark.**

The equations considered in the text are special cases of a nonlinear diffusion equation of the form:

$$\Psi_t = \phi(x)a^{ij}(\nabla\Psi)\partial_{ij}\Psi + H(x, \nabla\Psi), \quad x = (x_1, \dots, x_n). \quad (23)$$

As in [3, 7, 13], under mild hypotheses obeyed by our contour models, one may show that

**Theorem 1** *There is a unique viscosity solution of (23) in  $L^\infty(0, T; W^{1,\infty}(\mathbf{R}^n))$ .*

## 6 Examples

An important consideration for the numerical simulation of shape modelling flows is that for any  $t$  the image-based stopping term  $\phi$  has proper meaning only on the zero level set of the embedding surface  $\Psi$ . In order to extend this influence to other level sets we use the narrow band technique of [19]. We compute the diffusive  $\phi$ -length minimizing component using central differences and the hyperbolic  $\phi$ -area minimizing one using upwind schemes.

As observed in [13] a difficulty with using a large constant motion force  $\nu$  (which is desirable for fast convergence) in equation (15) is that it may cause overshooting of the edge since  $\phi$  may not be rigorously zero on the contour to be captured. The stopping behavior of the  $\langle \nabla\phi, \nabla\Psi \rangle$

term introduced in [8, 13, 14, 26] can help by arresting the evolution of the front in the vicinity of edges. However, in our experience with comparative simulations between this last technique and our combined  $\phi$ -length and  $\phi$ -area minimizing flow, we have found that the latter offers at least two advantages. First, the hyperbolic component of the flow is now *adaptive*, adjusting itself according to the local gradient of the scalar potential  $\phi$  in the vicinity of the evolving curve  $\mathcal{C}$ . Second, the doublet term  $\langle \nabla \phi, \mathcal{C} \rangle$  in (17) provides an additional attraction force in the vicinity of edges, allowing for a larger weight to be assigned to the  $\phi$ -area component of the flow.

We consider several examples of shape segmentation using the 2D medical images shown in Figure 1: a 256x256 MRI section of a brain, a 256x256 MRI image showing the short axis view of a heart, and a 276x268 CT image of a bone<sup>2</sup>. For all simulations  $\phi$  was constructed as in (16), but with curvature based smoothing of the original image [4, 15], with  $n = 2$  for the MRI images and  $n = 4$  for the CT image.

Figures 2 and 3 depict the segmentation of the brain and heart ventricles, respectively, with the evolving curve overlaid in white on the curvature smoothed original. Observe that for each image the front converges on the desired boundary. We should note that when run with the same parameters ( $\Delta t$ , and the weights for the parabolic and hyperbolic components), the flow of [8, 13, 14, 26] produces comparable results.

The advantages of using the  $\phi$ -area component emerge when the above flows are applied to the more difficult CT bone image, again using identical parameters<sup>3</sup>. Observe that whereas our new flow converges on the desired boundary, Figure 4 (left), the flow of [8, 13, 14, 26] eventually “leaks” through, Figure 4 (right).

Next, using the same parameters as in Figure 2, we examine the efficacy of using only the  $\phi$ -area component for segmentation in Figure 5, under three different initial conditions. This offers significant computational savings because only first-order derivatives have to be computed. Also, in most cases the front converges in fewer iterations since it is no longer constrained to remain smooth. We note that although the evolution is not translation invariant due to the doublet term  $\langle \nabla \phi, \mathcal{C} \rangle$ , the final segmentations in Figures 5 a) and 5 b) are basically identical except for the piece of noise captured in the latter. This is due to the simple fact that in case (a) the structure

---

<sup>2</sup>The CT bone image is contrast normalized for display purposes since the original has pixel values ranging only from 0 to 38.

<sup>3</sup>Note that here the direction of the hyperbolic component has been reversed, so it is actually a  $\phi$ -area maximizing flow.

was not enclosed, while in case (b) it was enclosed by the initial contour. The length minimizing component has some advantage for such “pieces of noise” since typically they are small structures of high curvature, through which the additional length minimizing component would push through.

Finally, in Figure 6 we compare segmentation using the  $\phi$ -area component against segmentation with pure constant motion (*i.e.* without the doublet term) in the presence of gaps, such as those caused by blurred edges. The simulations illustrate that whereas the doublet term does add a degree of robustness when the gaps are small, in the presence of larger gaps the  $\phi$ -area flow will eventually leak through. In such situations, the contribution of the  $\phi$ -length component is critical.

## 7 Conclusions

Curvature flows have proven to be a powerful tool for a variety of problems in image processing and computer vision. In this paper we have proposed a conformal area based gradient flow for image segmentation and edge finding. This is to be used in conjunction with the conformal length based gradient flows already proposed in the literature [8, 13, 14, 26]. As such, we believe that we now have a rather complete picture for the use of such curvature-driven evolution equations for segmentation. Experiments must still be run to study the efficacy of the new flow for volumetric imagery.

On the level of shape representation, our flow can be regarded as defining a “conformal skeleton.” Indeed, we have been recently employing this flow for a theory of *hyperbolic smoothing of shapes*, and to define a new “reaction-diffusion” space for planar shape representation. The idea is to use the stopping term to hierarchically remove noise before letting the hyperbolic morphological component take over. This work will be described in our paper [27].

**Acknowledgements** The authors would like to thank the referees for their very helpful comments. This work was supported by grants from the Natural Sciences and Engineering Research Council of Canada, from the National Science Foundation, from the Air Force Office of Scientific Research and from the Army Research Office.

## References

- [1] L. Alvarez, F. Guichard, P. L. Lions, and J. M. Morel. Axiomatisation et nouveaux opérateurs de

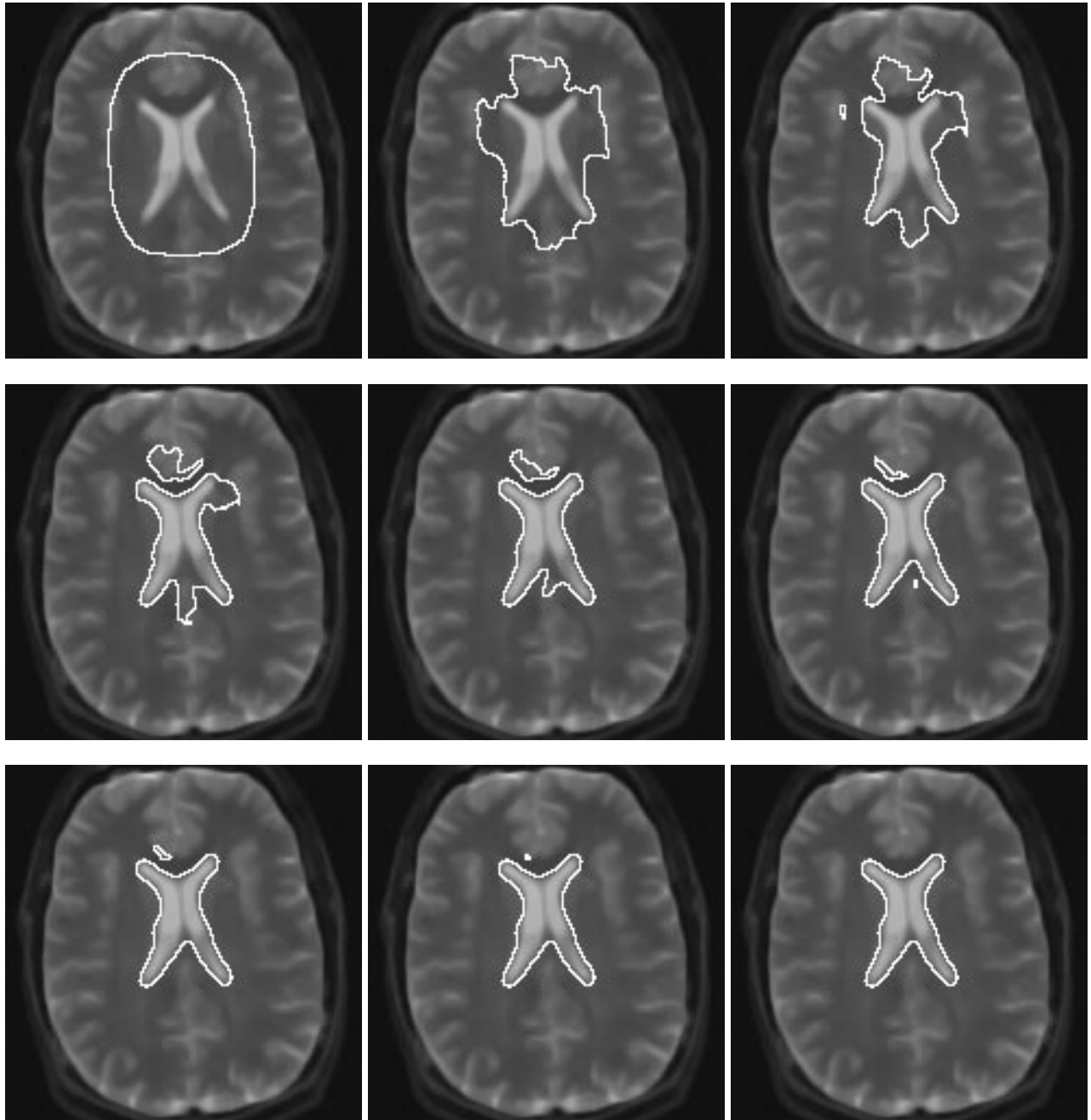


Figure 2: The front evolving under equation (17), overlaid in white, converges on the outline of the brain ventricle. TOP TO BOTTOM, LEFT TO RIGHT: iterations 1,200,400,600,800,1000,1200,1400, and 1600.

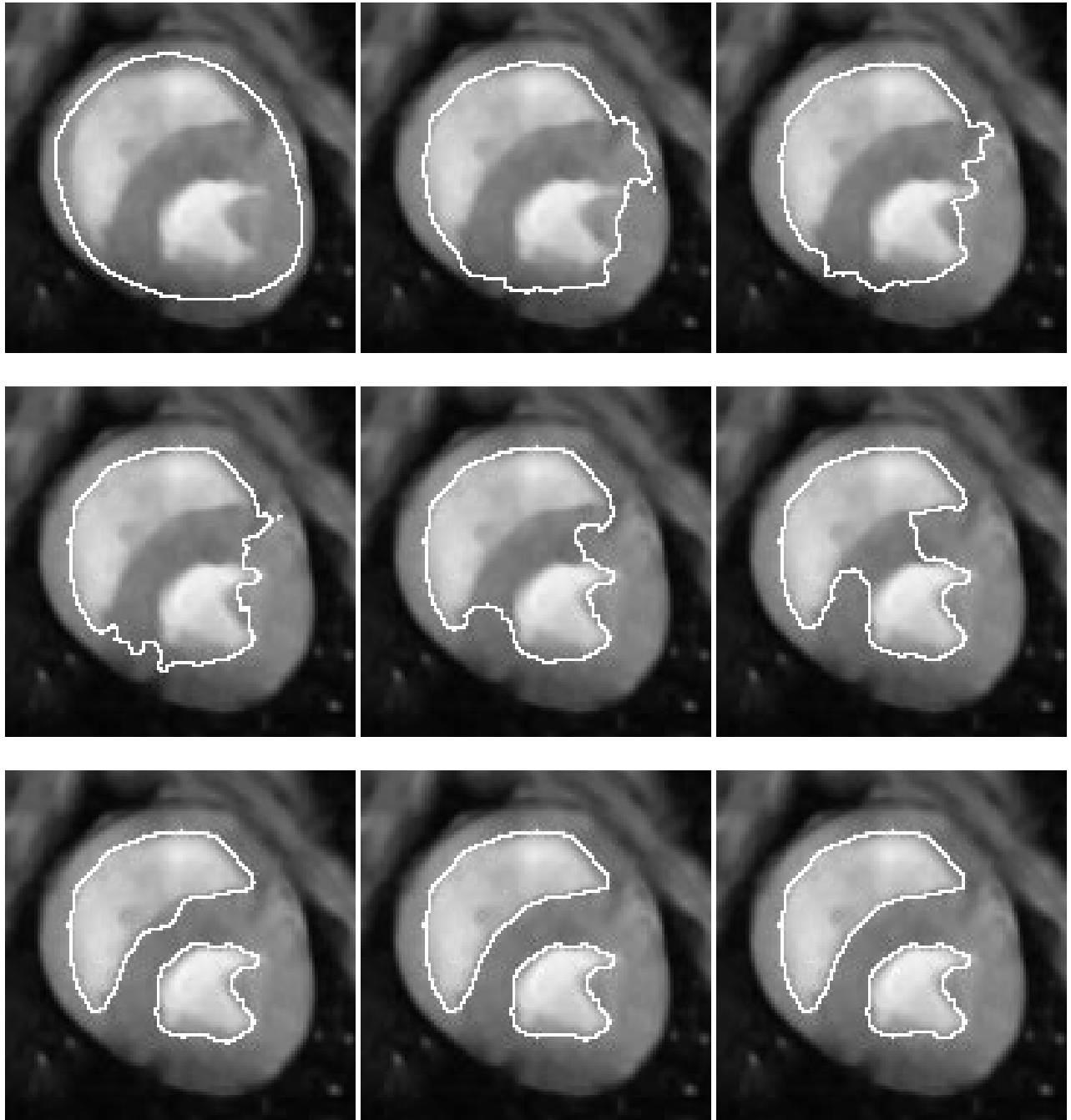


Figure 3: The front evolving under equation (17), overlaid in white, converges on the ventricles of the heart. TOP TO BOTTOM, LEFT TO RIGHT: iterations 1,200,400,600,800,1000,1200,1400, and 1600.

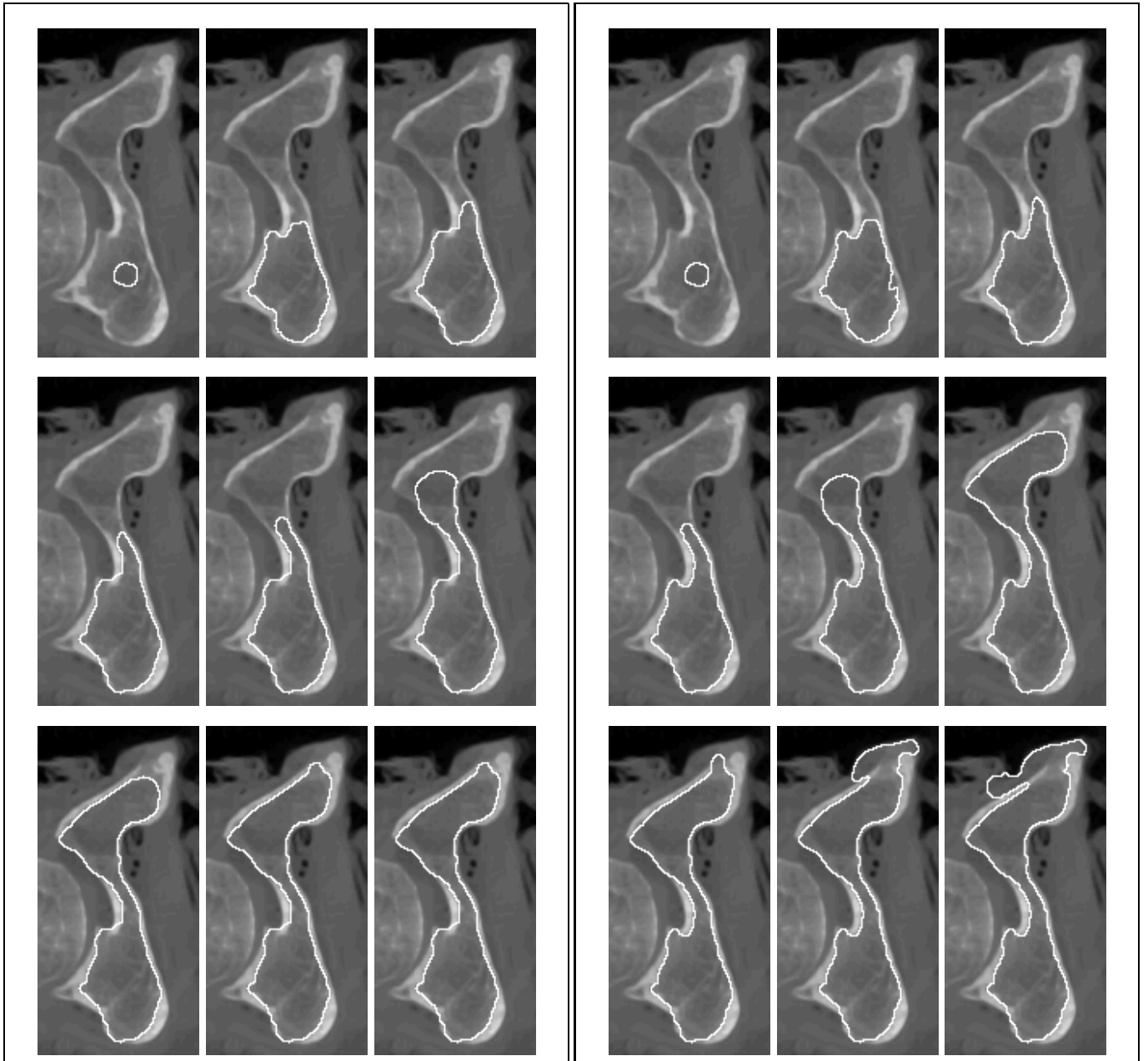


Figure 4: Reversing the direction of the hyperbolic component, the front evolving under equation (17), overlaid in white, converges on the outline of the bone (LEFT). Using identical parameters, the flow of [8, 13, 14, 26] eventually “leaks” through (RIGHT). TOP TO BOTTOM, LEFT TO RIGHT: iterations 1,250,500,750,1000,1250,1500,1750, and 2000.

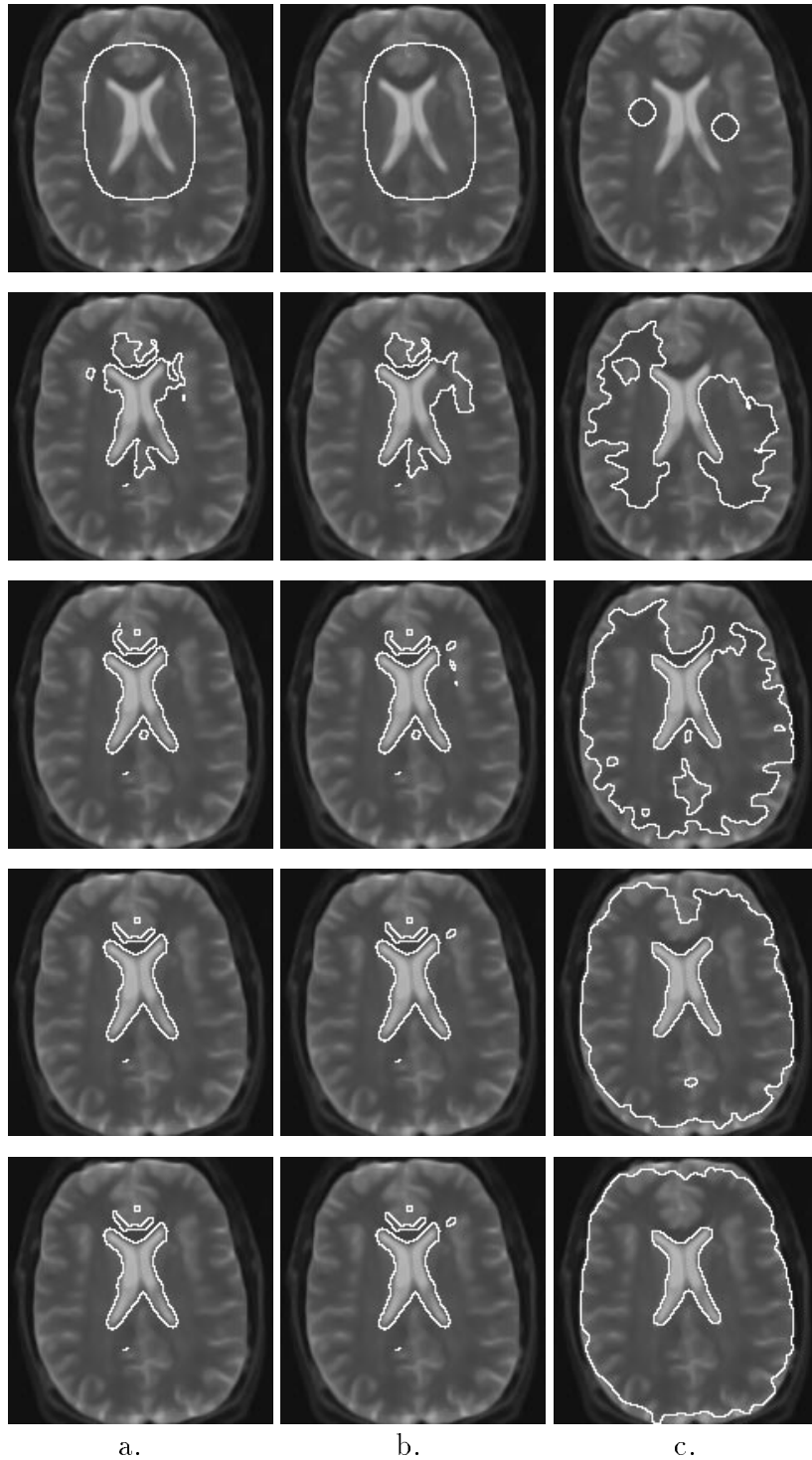


Figure 5: Segmentation of the brain ventricle using only the weighted area term of equation (17). In a) the same initial curve is used as in Figure 2, in b) the initial curve is translated, and in c) an entirely different initial condition is used and the direction of the flow is reversed. TOP TO BOTTOM: iterations 1,400,800,1200,1600.

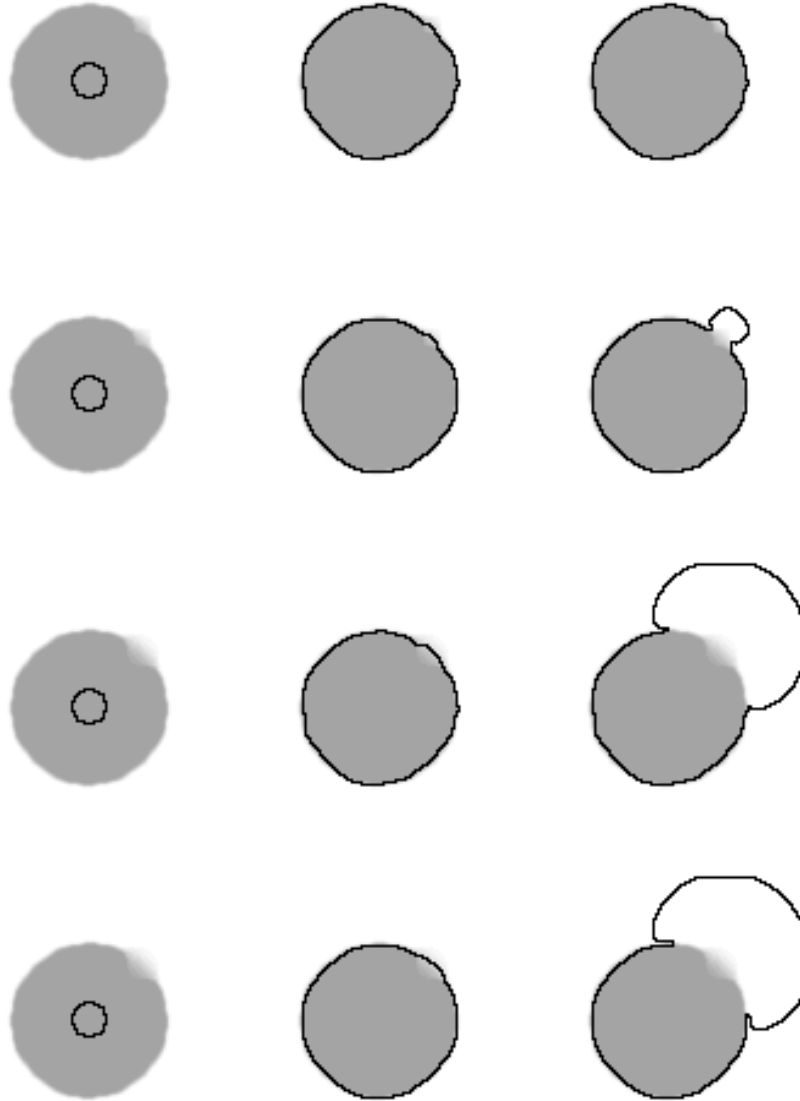


Figure 6: A comparison of segmentation by the weighted area term of equation (17), and segmentation by a pure constant inflation term (*i.e.* without the doublet). The synthetic images consist of a disk of intensity 100 on a background of intensity 125, with Gaussian blur applied to an edge. When the blur is restricted to a  $7 \times 7$  region, the doublet term is strong enough to arrest the front (TOP ROW), whereas without it the front passes through (SECOND ROW). However, when the blur is applied to a larger  $13 \times 13$  region, the front passes through for both cases (THIRD AND FOURTH ROWS). LEFT TO RIGHT: iterations 1,253,541.

- la morphologie mathématique. *C. R. Acad. Sci. Paris*, 315:265–268, 1992.
- [2] L. Alvarez, F. Guichard, P. L. Lions, and J. M. Morel. Axiomes et équations fondamentales du traitement d’images. *C. R. Acad. Sci. Paris*, 315:135–138, 1992.
- [3] L. Alvarez, F. Guichard, P. L. Lions, and J. M. Morel. Axioms and fundamental equations of image processing. *Archive of Rational Mechanics and Analysis*, 123, 1993.
- [4] L. Alvarez, P. L. Lions, and J. M. Morel. Image selective smoothing and edge detection by nonlinear diffusion. *SIAM J. Numer. Anal.*, 29:845–866, 1992.
- [5] A. Blake and A. Yuille. *Active Vision*. MIT Press, Cambridge, Mass., 1992.
- [6] M. P. D. Carmo. *Riemannian Geometry*. Birkhauser, 1992.
- [7] V. Caselles, F. Catte, T. Coll, and F. Dibos. A geometric model for active contours in image processing. *Numerische Mathematik*, 66:1–31, 1993.
- [8] V. Caselles, R. Kimmel, and G. Sapiro. Geodesic active contours. In *Fifth International Conference on Computer Vision*, pages 694–699. IEEE Computer Society Press, 1995.
- [9] V. Caselles, R. Kimmel, G. Sapiro, and C. Sbert. Minimal surfaces: A three dimensional segmentation approach. Technical Report 973, Technion, June 1995.
- [10] M. Gage and R. Hamilton. The heat equation shrinking convex plane curves. *J. Diff. Geom.*, 23:69–96, 1986.
- [11] M. Grayson. The heat equation shrinks embedded plane curves to round points. *J. of Differential Geometry*, 26:285–314, 1987.
- [12] M. Kass, A. Witkin, and D. Terzopoulos. Snakes: Active contour models. *Int. Journal of Computer Vision*, 1:321–331, 1987.
- [13] S. Kichenassamy, A. Kumar, P. Olver, A. Tannenbaum, and A. Yezzi. Gradient flows and geometric active contour models. In *Fifth International Conference on Computer Vision*, pages 810–815. IEEE Computer Society Press, 1995.
- [14] S. Kichenassamy, A. Kumar, P. Olver, A. Tannenbaum, and A. Yezzi. Conformal curvature flows: From phase transitions to active vision. *Archives of Rational Mechanics and Analysis*, 134:275–301, 1996.

- [15] B. B. Kimia and K. Siddiqi. Geometric heat equation and non-linear diffusion of shapes and images. *Computer Vision and Image Understanding*, 64(3):305–322, 1996.
- [16] B. B. Kimia, A. Tannenbaum, and S. W. Zucker. Toward a computational theory of shape: An overview. *Lecture Notes in Computer Science*, 427:402–407, 1990.
- [17] B. B. Kimia, A. Tannenbaum, and S. W. Zucker. On the evolution of curves via a function of curvature I: The classical case. *J. of Math. Analysis and Applications*, 163:438–458, 1992.
- [18] B. B. Kimia, A. Tannenbaum, and S. W. Zucker. Shape, shocks, and deformations I: The components of two-dimensional shape and the reaction-diffusion space. *Int. J. Computer Vision*, 15:189–224, 1995.
- [19] R. Malladi, J. A. Sethian, and B. C. Vemuri. Shape modeling with front propagation: A level set approach. *IEEE Transactions on Pattern Analysis and Machine Intelligence*, 17(2):158–175, February 1995.
- [20] P. Olver, G. Sapiro, and A. Tannenbaum. Affine invariant edge maps and active contours. *CVIU*, submitted for publication.
- [21] S. Osher. Riemann solvers, the entropy condition, and difference approximations. *SIAM J. Numer. Anal.*, 21:217–235, 1984.
- [22] G. Sapiro and A. Tannenbaum. On affine plane curve evolution. *Journal of Functional Analysis*, 119:79–120, 1994.
- [23] J. A. Sethian. *An Analysis of Flame Propagation*. PhD thesis, University of California, 1982.
- [24] J. A. Sethian. Curvature and the evolution of fronts. *Commun. Math. Phys.*, 101:487–499, 1985.
- [25] J. A. Sethian. A review of recent numerical algorithms for hypersurfaces moving with curvature dependent speed. *J. of Differential Geometry*, 31:131–161, 1989.
- [26] J. Shah. Recovery of shapes by evolution of zero-crossings. Technical report, Dept. of Mathematics, Northeastern University, Boston, MA, 1995.
- [27] K. Siddiqi, Y. B. Lauzière, A. Tannenbaum, and S. W. Zucker. Hyperbolic smoothing of shapes. *In preparation*, 1996.
- [28] H. Tek and B. Kimia. Deformable bubbles in the reaction-diffusion space. In *Fifth International Conference on Computer Vision*. IEEE Computer Society Press, 1995.

- [29] D. Terzopoulos and A. Witkin. Constraints on deformable models: Recovering shape and non-rigid motion. *Artificial Intelligence*, 36:91–123, 1988.
- [30] A. Yezzi, S. Kichenessamy, A. Kumar, P. Olver, and A. Tannenbaum. A geometric snake model for segmentation of medical imagery. *IEEE Trans. on Medical Imaging*, to appear.